Adding interferometry for CMBPol

Peter Timbie[1] **and Greg Tucker**[2]

[1] Department of Physics, University of Wisconsin, Madison, WI 53706
[2] Department of Physics, Brown University, Providence RI 02912

E-mail: pttimbie@wisc.edu, gst@brown.edu

Abstract. Interferometry offers an alternative to imaging of the CMB. Some systematic errors may be easier to control than in the imaging case. Adding interferometry is capable of correlating signals from a large number of antennas, more than is currently possible with traditional multiplying interferometers. Many of the technologies required for a space-based adding interferometer for CMB studies are the same as for imaging systems. We evaluate those critical components which are different from imagers.

1. Introduction

Interferometers have been used for many years for studying the CMB temperature and polarization power spectra and the Sunyaev-Zel'dovich effect. In fact, the first detection of CMB E-mode polarization was made by an interferometer: DASI [1]. There are many reasons to consider using interferometers for measurements of the B-mode signal. The key reason is to control systematic effects.

Recently, several groups have studied the possibility of building future interferometers specifically to search for the small polarization signals in the CMB. Compared to existing interferometers, these new instruments would have to: 1) collect more modes of radiation from the sky by adding more (single-mode) antennas and 2) operate over a broader range of frequencies, at least up to 90 GHz, and 3) with broader bandwidth, to be able to detect and reject astrophysical foreground sources. The most significant challenge to increasing the number of antennas is correlating the large number of baselines. There are two approaches: *multiplying* interferometry and *adding* interferometry.

Other white papers for this workshop will address means of applying traditional multiplying interferometry (sometimes called heterodyne interferometry because the RF signal is typically mixed to a lower frequency before the correlator) to the B-mode search. These methods use coherent receivers (SIS or HEMT) and are currently limited by the correlator, both in bandwidth and number of baselines. We focus here on adding interferometers, which have the ability to use either coherent or incoherent detectors (bolometers) and for which correlators with large bandwidths and large numbers of inputs appear feasible.

We focus on systems that provide modest angular resolution ($\sim 1^\circ$) and large fields of view ($\sim 10^\circ$), appropriate for measurements of the recombination and reionization peaks in the B-mode power spectrum. In this case a compact interferometer array can be formed from a cluster of circular horn antennas (similar to DASI).

2. History and Advantages of Interferometry

Interferometers have proved to be powerful tools for CMB observations (see [2] for a comprehensive list). The Sunyaev-Zel'dovich effect has been imaged by the Ryle [3], OVRO and BIMA interferometers [4] and the SZA [5] at centimeter wavelengths. The CMB temperature anisotropy has been imaged by the CAT [6], VSA [7], DASI [8] and CBI [9] interferometers, also at centimeter wavelengths. DASI was the first instrument to detect the CMB polarization [1; 10] and CBI has detected CMB polarization at smaller angular scales [11; 12]. These measurements were all made by "traditional" interferometers that use coherent receivers and correlate signals from each pair of antennas in the array by multiplying the amplified electric fields together. The correlated signals form the visibility. There are $N(N-1)/2$ such pairs (baselines).

The main reason for building interferometers instead of traditional imaging systems for studying the CMB is to control systematic effects, which in some cases are more manageable than in imaging systems. There are additional factors, especially aperture size, that favor interferometric approaches over imaging for space-based systems.

2.1. Angular Resolution

For a monolithic dish of diameter, D, equal to the length of a two-element interferometer baseline, B, the interferometer has angular resolution (fringe spacing) roughly twice as good as that of the monolithic dish. The reason for this difference in angular resolution is that the filled dish is dominated by spacings that are much smaller than the aperture diameter. The full width to the first zero for a uniformly illuminated circular aperture of diameter D is $2.4\lambda/D$. The full width to the first zero for a two-element interferometer, when the baseline B is much larger than the individual aperture diameter, is λ/B. It is helpful to consider the difference between the systems in l-space as well. For an interferometer the window function peaks at $l = 2\pi B/\lambda$. For an imaging system with a Gaussian beam the window function is $W_l = e^{-l^2\sigma^2}$. The beamwidth $\sigma = 0.42$ FWHM and FWHM $= (1.02+0.0135T_e)\lambda/D$ where T_e is the edge taper of the antenna in dB [13]. For an edge taper of 40 dB (typical for CMB instruments), FWHM $= 1.51\lambda/D$, $\sigma = 0.66\lambda/D$ and the window function falls to 10% of its peak value at $l = 2.29D/\lambda$, which is less than half of the peak l-value for an interferometer baseline of the same size.

This angular resolution factor is important because the size of the aperture is a cost-driver for the CMBPol mission. Angular resolution is important for CMB polarization measurements in two ways. First, imperfections in the shape and pointing of beams couple the CMB temperature anisotropy into false polarization signals. These problems can be reduced significantly if the CMB is smooth on the scale of the beam size, which happens for beams smaller than $\sim 10'$ [14]. Second, removing contamination of the tensor B-mode signal by B-modes from weak lensing requires maps of the lensing at higher angular resolution than the scale at which the tensor B-modes peak [15].

2.2. No Rapid Chopping and Scanning

Imaging systems with either coherent or incoherent detectors typically use some form of "chopping," either by nutating a secondary mirror or by steering the entire primary at a rate faster than the $1/f$ noise in the atmosphere and detectors. Similar approaches are used with arrays of detectors. When using an imaging system to form a two-dimensional (2D) map with minimal striping or other artifacts, the scan method must move the beam (or beams) on the sky at a rapid rate. Interferometers provide direct 2D imaging and do not require such scanning strategies. In the interferometer, only correlated signals are detected, so it has reduced sensitivity to changes in the total power signal absorbed by the detectors [16].

Table 1. Comparison of various optical designs for CMBPol. To achieve the same angular resolution each instrument allows different amounts of throughput (number of modes) and requires different aperture diameters, D. For the Gregorian the edge taper on the primary mirror illumination is assumed to be -40dB, the diameter of the FOV is given in degrees and the number of modes is approximately [FOV/(angular resolution)]^2, assuming all the modes reaching the focal plane are coupled to detectors. For the imaging horn array, the horn diameter $= D$. For the interferometric horn array, $D = B$, the diameter of a close-packed array of horns, each of diameter d, and the number of modes is given by the number of horns $\sim (D/d)^2$. In the last three columns, for all cases, the angular resolution $= 1^\circ$ and $\lambda = 3$ mm.

Instrument	*Angular resolution* (FWHM)	*FOV* ($^\circ$)	*Aperture D* (cm)	*Modes*
Gregorian telescope	$1.51\lambda/D$	~ 7	26	49
Imaging horn array	$2\lambda/D$	$2\lambda/D$	34	1
Interfer. horn array	$\lambda/2D$	$2\lambda/d$	8.6	16

2.3. Clean Optics

The simplicity of an interferometric optical system eliminates numerous systematic problems that plague imaging optical systems. Instead of a single reflector antenna, the interferometers discussed here use arrays of corrugated horn antennas. These antennas have extremely low sidelobes and have easily calculable, symmetric beam patterns. Furthermore, there are no reflections from optical surfaces to induce spurious instrumental polarization, an unavoidable problem for any system with imaging optics [17; 18]. In principle, one could construct an imaging instrument without reflective optics; an array of horn antennas, each coupled directly to a polarimeter, could view the sky directly. Each horn aperture would be sized to provide the required angular resolution. However, such a system uses the aperture plane inefficiently. A single horn antenna in such an imaging system will have angular resolution $\sim 2\lambda/D$, where D is the horn diameter. An N - element interferometric horn array that achieves the same angular resolution will have a maximum baseline length of $B = D$ (and require the same aperture size), but will collect N modes of radiation from the sky and hence be more sensitive.

Another advantage over an imaging system is the absence of aberrations from off-axis pixels: all feed elements are equivalent for the interferometer. In contrast to an imaging system, the field-of-view (FOV) of an interferometer is determined by the primary beamwidth of the array elements, not by beam distortion and cross-polarization at the edge of the focal plane. One can choose to increase the sensitivity of the instrument by collecting more modes (optical throughput) of radiation from the sky. In the interferometer this can be done by adding additional antennas; the only limitation is the size of the aperture plane rather than optical aberrations in the focal plane. The largest usable FOV for an off-axis Gregorian reflector is approximately 7° [19]. See Table 1 for a comparison of imaging and interferometric optical systems.

2.4. Direct Measurement of Stokes Parameters

Interferometry solves many of the problems related to mismatched beams and pointing errors raised by [14]. This advantage arises because interferometers measure the Stokes parameters directly, without differencing the signal from separate detectors.

An interferometer measures the Stokes parameters by correlating the components of the electric field captured by each antenna with the components from all of the other antennas. If

the output of each antenna is split into E_x and E_y by an orthomode transducer (OMT), on the baseline formed by two antennas, 1 and 2, the interferometer's correlators measure $\langle E_{1x}E_{2x}\rangle$, $\langle E_{1y}E_{2y}\rangle$, $\langle E_{1x}E_{2y}\rangle$, and $\langle E_{1y}E_{2x}\rangle$. The first two are used to determine I and the latter two measure U. Rotating the instrument allows a measurement of Q. Stokes V can be recovered in a similar manner. Alternatively, the antenna outputs can be separated into left- and right-circular polarization components by a combination of an OMT and a polarizer. Correlating these signals also allows recovery of all four Stokes parameters. DASI uses a switchable polarizer to accomplish this [20].

[14] have reviewed systematic effects relevant to CMB polarization measurements, mainly in the context of imaging instruments. [21] performs similar calculations for interferometers. Table 2 outlines a variety of systematic errors and how they can be managed in imaging and infererometric instruments. The relative importance of these effects is quite different in interferometric systems: some sources of systematic error in imaging systems are dramatically reduced in interferometers. As an example we consider the effects of pointing errors and mismatched antenna patterns.

Some imaging instruments used for CMB polarization measure the power in each linear polarization on separate bolometers and then form the difference of the two signals to determine the linear polarization. This approach requires careful matching of the bolometers. Moreover, if the signals being differenced come from two different antennas, then the beam patterns and pointing of the two antennas must coincide precisely. Any mismatch converts power from the total intensity into a spurious polarization signal [14]. In an interferometer, differences in antenna patterns for the different horns do not couple intensity to polarization in this way (see below).

In a traditional imaging system, the Stokes parameters Q and U are determined by subtracting the intensities of two different polarizations. For example, Q might be measured by splitting the incoming radiation into x and y polarizations, determining the intensities I_x and I_y of the two polarizations, and subtracting. In such an experiment, any mismatch in the beam patterns used to determine I_x and I_y (including differential pointing errors as well as different beam shapes) will cause leakage from total power (T) into polarization (Q, U).

In an interferometer, the signals are combined before squaring to get intensities. In such a system, mismatched beams do not lead to leakage from temperature into polarization. Suppose that the signal entering each horn of an interferometer is split into horizontal and vertical polarizations. Working in the flat-sky approximation, let $E_{ix}(\hat{r})$ and $E_{iy}(\hat{r})$ stand for the x and y components of the electric field of the radiation entering the ith horn from position $\hat{r}$ on the sky. The signals coming out of each horn are averages of the incoming electric fields weighted by some antenna patterns $G_{i(x,y)}(\hat{r})$.

In an interferometer, these signals are multiplied together to obtain a visibility. To measure the Stokes parameter U, for example, we would multiply the x signal from horn i with the y signal from horn j to obtain the visibility

$$V_{ij}^U = \int d\hat{r}_1\, d\hat{r}_2\, G_{ix}(\hat{r}_1) G_{jy}(\hat{r}_2) \langle E_{ix}(\hat{r}_1) E_{jy}^*(\hat{r}_2)\rangle.$$

The angle brackets denote a time verage. The electric fields due to radiation coming from two different points on the sky are uncorrelated, and the product of x and y components of the electric field gives the Stokes U parameter:

$$\langle E_{ix}(\hat{r}_1) E_{jy}^*(\hat{r}_2)\rangle = U(\hat{r}_1) e^{2\pi i \vec{u}\cdot\hat{r}_1} \delta(\hat{r}_1 - \hat{r}_2),$$

so the visibility is

$$V_{ij}^U = \int d\hat{r} G_{ix}(\hat{r}) G_{jy}(\hat{r}) U(\hat{r}) e^{2\pi i \vec{u}\cdot\hat{r}}.$$

Table 2. A Comparison of Systematic Effects

Systematic Effect	*Imaging System Solution*	*Interferometer Solution*
Cross-polar beam response	Instrument rotation & correction in analysis	Instrument rotation & non-reflective optics
Beam ellipticity	Instrument rotation & small beamwidth	No T to E and B leakage from beams; inst. rot'n
Polarized sidelobes	Correction in analysis	Correction in analysis
Instrumental polarization	Rotation of instrument & correction in analysis	Clean, non-reflective optics
Polarization angle	Construction & characterization	No T to E and B leakage from beams; construction & characterization
Relative pointing	Rotation of instrument & dual polarization pixels	No T to E and B leakage from beams; inst. rot'n
Relative calibration	Measure calibration using temperature anisotropies	Detector comparison not req'd for mapping or measuring Q and U
Relative calibration drift	Control scan-synchronous drift to 10^{-9} level	All signals on all detectors
Optics temperature drifts	Cool optics to $\sim$3 K & stabilize to $< \mu$K	No reflective optics
$1/f$ noise in detectors	Scanning strategy & phase modulation/ lock-in	Instant. measurement of power spectrum without scanning
Astrophysical foregrounds	Multiple frequency bands	Multiple frequency bands

Note that the visibility V_{ij}^U does not contain any contribution from the total intensity (Stokes I), *even if* the two antenna patterns are different. This means that differential pointing errors and different beam shapes for different antennas do not cause leakage from T into E and B. Antenna pattern differences do cause distortion of the observed polarization field, so errors in modeling beam shapes and pointing may cause mixing between E and B.

Coupling between intensity and polarization will arise if the beams have cross-polar contributions. In that case, the visibility V_{ij}^U, which is supposed to be sensitive to just polarization, will contain contributions proportional to $\langle E_x E_x^* \rangle$ and $\langle E_y E_y^* \rangle$, to which Stokes I does contribute.

The same considerations apply if the incoming radiation is split into circular rather than linear polarization states. The visibility V_{ij}^{RL}, obtained by interfering the right-circularly-polarized signal entering horn i with the left-circularly-polarized signal entering horn j, contains only contributions from Q and U if the beams are co-polar, even if the two horns have different beams. Again, cross-polarity induces leakage from intensity into polarization.

In short, in an interferometer, beam mismatches are less of a worry than for imaging systems.

2.5. Separation of E and B Modes

A significant challenge in CMB polarization measurements is separation of the very weak B modes from the much stronger E modes. Unless a full-sky map is made with infinite angular resolution the two modes "leak" into each other [22; 23]. It has been shown [24; 25], however,

that an interferometer can separate the E and B modes more cleanly than can an imaging experiment although detailed calculations of this advantage in realistic simulations remain to be done.

2.6. Foreground Removal

Foreground removal can occur in visibility space. Removing foregrounds directly from visibility data has been studied in another context [26]. CMBPol will undoubtedly have to measure foregrounds itself, without relying on other instruments. A set of interferometer modules scaled in proportion to wavelength and operating from ~ 30 to 300 GHz would provide a set of visibility measurements with identical $u - v$ coverage so that foregrounds could be studied and removed in visibility space.

3. Multiplying Interferometry

In a simple 2-element radio interferometer, signals from two telescopes aimed at the same point in the sky are correlated so that the sky temperature is sampled with an interference pattern with a single spatial frequency. The output of the multiplying interferometer is the visibility (defined in the last section). With more antennas these same correlations are performed along each baseline. To recover the full phase information, complex correlators are used to measure simultaneously both the in-phase and quadrature-phase components of the visibility. All interferometers used for CMB studies so far are multiplying interferometers and use use coherent receivers. They can use either analog or digital correlators.

Analog correlators. DASI and CBI use analog correlators. They first amplify the RF signals from each of the N antennas, downconvert in frequency with a mixer, and then split the signals $N - 1$ ways. The correlator then combines these signals in a pairwise fashion to measure visibilities for $N(N-1)/2$ baselines. For DASI and CBI $N = 13$, and the number of baselines is 78. But for $N = 100$, however, there would be 4950 baselines and this type of correlator is not yet feasible (although correlators could be made to correlate only a fraction of the possible baselines).

Digital correlators. See white papers by Ruf and Church in coherent task.

4. Adding Interferometry: Overview

An alternate approach is to use adding interferometry. Adding interferometry has the advantage that beam combiners that can be scaled to large bandwidths and large N are feasible and either coherent receivers or incoherent detectors (bolometers) can be used. Bolometers have the advantage of operating over the entire range of millimeter wavelengths of interest for CMB studies. In addition, they have comparable sensitivity to coherent receivers below ~ 90 GHz and better sensitivity at higher frequencies. The high-frequency sensitivity advantage improves in low background environments (balloons and space). When used without amplifiers, the main challenge to adding interferometry is combining the signals from the multiple antennas without sacrificing signal-to-noise. The beam combination is necessarily performed by analog correlators. These can be of two types, either "pairwise" or "all on one" combiners.

In adding interferometers the electric field wavefronts from two antennas are added and then squared in a detector [27]. (See Figure 1.) The result is a constant term proportional to the intensity plus an interference term. The constant term is an offset that is removed by phase-modulating one of the signals. Phase-sensitive detection at the modulation frequency recovers both the in-phase and quadrature-phase interference terms and reduces susceptibility to low-frequency drifts ($1/f$ noise) in the detector and readout electronics. The adding interferometer recovers the same visibility as a multiplying interferometer.

In an interferometer with an array of $N > 2$ antennas, the signals are combined in such a way that interference fringes are measured for all possible baselines ($N(N-1)/2$ antenna pairs). This

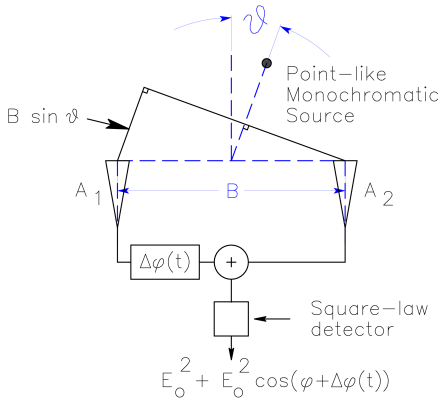

Figure 1. Adding interferometer with $N = 2$ antennas. At antenna A_2 the electric field is E_0, and at A_1 it is $E_0 e^{i\phi}$, where $\phi = kB \sin\alpha$ and $k = 2\pi/\lambda$. B is the length of the baseline, and α is the angle of the source with respect to the symmetry axis of the baseline, as shown. (For simplicity consider only one wavelength, λ, and ignore time dependent factors.) In a multiplying interferometer the in-phase output of the correlator is proportional to $E_0^2 \cos\phi$. For the adding interferometer, the output is proportional to $E_0^2 + E_0^2 \cos(\phi + \Delta\phi(t))$. Modulation of $\Delta\phi(t)$ allows the recovery of the interference term, $E_0^2 \cos\phi$, which is proportional to the visibility of the baseline.

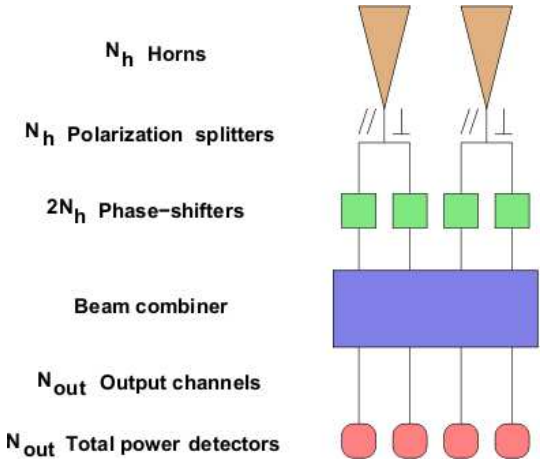

Figure 2. Block diagram of an adding interferometer that can be expanded to $N > 2$. Each phase shifter is modulated in a sequence that allows recovery of the interference terms (visibilities) by phase-sensitive detection at the detectors. The signals are mixed in the beam combiner and detected. The beam combiner can be implemented either using guided waves (Butler combiner) or quasioptically (Fizeau combiner, see below). The triangles represent corrugated conical horn antennas. Orthomode transducers (OMTs) allow all the Stokes parameters to be determined simultaneously. For the case of an interferometer using coherent receivers, amplifiers and/or mixers could be placed before the beam combiner. (Figure courtesy of Charlassier *et al. 2008* [29].)

combination can occur in two different ways: pairwise combination (analogous to a Michelson stellar interferometer) or all-on-one (Fizeau or Butler) combination [28].

Pairwise combination involves splitting the power from each of the N antennas in the array $N-1$ ways, adding the signals in a pairwise fashion, and then squaring the signals and separating out the interference term as described above. In optical systems this approach is analogous to Michelson stellar interferometry. This approach has the disadvantages of producing extremely low signal levels at each detector and requiring $N(N-1)/2$ extremely sensitive detectors.

In Fizeau or Butler combination the signals from each of the antennas are split and then combined in such a way that linear combinations of all the antenna signals are formed at each of the outputs of the combiner (Figure 2). This scheme avoids the problem of large numbers of detectors and low signal levels. To allow all the Stokes parameters to be determined simultaneously, orthomode transducers (OMTs) are inserted after the antennas. In this case, the Butler combiner delivers the signals from $2N$ antenna outputs to $2N$ detectors. Each detector squares these amplitudes, creating interference signals from all baselines simultaneously on each detector. Effectively, the signals from all baselines are multiplexed onto each of the $2N$ detectors. Only $2N$ detectors are required, rather than the $2N(2N-1)/2$ detectors required for pairwise combination. Butler combiners are commonly used for phased array antennas with coherent systems using either waveguide or coaxial techniques. The optical analog is Fizeau combination, which is typically used for incoherent systems at optical wavelengths and has lower loss than Butler combiners. In a coherent system, with amplifiers, the Butler approach is still an attractive

option for forming a large-N interferometer.

In the Fizeau/Butler approach, the signals from redundant baselines can be added together to improve the signal - to - noise ratio at each bolometer compared to the pairwise combination case [29]. The signals reaching each bolometer are multiplexed in such a way that a portion of the visibility of each baseline appears at each bolometer. When the signals are combined the resultant sensitivity is comparable to that of a filled-dish with an array of bolometers coupled to the same number of modes (N) on the sky [30].

These systems actually interfere antenna signals in two modes of operation (see next section). In one mode, signals from different antennas are interfered to measure the visibility for each baseline. Each visibility selects a narrow range of l values and has no response to very low multipoles. In the second mode, signals from each antenna are combined with other signals from the same antenna (autocorrelation) to form a correlation polarimeter. This latter mode has lower angular resolution than the first, but is essential for measuring large spatial features (low-l).

5. Adding Interferometry: Details

Here we lay out the formalism needed to understand how the adding interferometer recovers the visibilities. Much of this section comes directly from Charlassier *et al. 2008* [29].

5.1. Horns

We assume that the instrument observes the sky through N_h input horns placed on an array at positions $\vec{d_i}$. All horn apertures are coplanar and look towards the same direction on the sky. They are characterized by their beam pattern on the sky noted $G(\hat{r})$ where $\hat{r}$ is the unit vector on the sphere. Two horns i and j form a baseline which we label by $0 \leq b \leq N_h(N_h-1)/2-1$. The phase difference between the signal reaching the two horns from the same direction $\hat{r}$ of the sky is such that:

$$E_j(\hat{r}) = E_i(\hat{r}) \exp(2i\pi \vec{u}_b \cdot \hat{r}), \text{ where } \vec{u}_b = (\vec{d_j} - \vec{d_i})/\lambda, \tag{1}$$

where λ is the central observing wavelength.

5.2. Equivalent baselines

It is clear that if two baselines b and b' are such that $\vec{u}_b = \vec{u}_{b'}$, then the phase shifts associated with the two baselines are equal, a fact that we shall extensively use in the following. All baselines b such that $\vec{u}_b = \vec{u}_\beta$ form a class of equivalent baselines associated with mode $\vec{u}_\beta$ in visibility space. For all baselines b belonging to the same class β, the phase difference between the two horns i and j is the same:

$$E_j(\hat{r}) = E_i(\hat{r}) \exp(2i\pi \vec{u}_\beta \cdot \hat{r}). \tag{2}$$

The number $N_{\neq}$ of different classes of equivalent baselines depends on the array, and the number of different baselines in an equivalence class also depends on the particular class.

5.3. Polarization splitters

There is an OMT at the output of each horn which separates the radiation into two orthogonal components noted $\parallel$ and $\perp$. Each horn therefore has two outputs measuring the electric field integrated through the beam in the two orthogonal directions. The contribution coming from direction $\vec{r}$ for polarization η ($\parallel$ or $\perp$) is:

$$\epsilon_i^\eta(\hat{r}) = G(\hat{r}) E_i^\eta(\hat{r}). \tag{3}$$

5.4. Phase-shifters

Phase-shifters placed on each of the outputs allow the phase of the electric field to be shifted by a given angle that can be chosen and controlled externally. This is the way the signal is modulated in order to recover the incoming information. For now we do not make any assumptions on the possible values of the angles but we will see that they have to be chosen carefully in order to optimize the signal to noise ratio. The signal after phase-shifting coming from direction $\hat{r}$ with polarization η is:

$$\epsilon_i'^{\eta}(\hat{r}) = \exp(i\phi_i^{\eta})\epsilon_i^{\eta}(\hat{r}). \tag{4}$$

5.5. Amplifiers

In the case of an adding interferometer that uses coherent receivers, low noise amplifiers (not shown in Fig. 2) would be placed before the beam combiner.

5.6. Beam combiner

For either a Butler or Fizeau combiner, $2N_h$ input channels are combined to create $N_{\rm out}$ output channels that are linear combinations of the inputs. To conserve the input power in an ideal lossless device, the number of output channels $N_{\rm out}$ has to be at least equal to the number of input channels $2N_h$. In the output channel k the electric field is:

$$z_k(\hat{r}) = \frac{1}{\sqrt{N_{\rm out}}} \sum_{i=0}^{N_h-1} \sum_{\eta=0}^{1} \gamma_{k,i}^{\eta} \epsilon_i^{\eta}(\hat{r}) \exp(i\phi_i^{\eta}), \tag{5}$$

where the $\gamma_{k,i}^{\eta}$ coefficient models the beam combiner, $\eta = 1$ or 0 respectively corresponds to $\parallel$ and $\perp$ polarizations. We choose to deal with configurations where the incoming power is equally distributed among all output channels, meaning that the coefficients $\gamma_{k,i}^{\eta}$ have a unit modulus: $\left|\gamma_{k,i}^{\eta}(k)\right| = 1$. In order to simplify the notation, we include the $\gamma_{k,i}^{\eta}$ phases in the phase-shifting terms as $\Phi_{k,i}^{\eta} = \phi_i^{\eta} + \mathrm{Arg}(\gamma_{k,i}^{\eta})$ so that:

$$z_k(\hat{r}) = \frac{1}{\sqrt{N_{\rm out}}} \sum_{i=0}^{N_h-1} \sum_{\eta=0}^{1} \epsilon_i^{\eta}(\hat{r}) \exp(i\Phi_{k,i}^{\eta}). \tag{6}$$

The beam combiner could be a Butler combiner, formed using guided waves (waveguides or planar transmission lines), or a Fizeau combiner using quasi-optical techniques. Butler combiners represent one of a large variety of guided wave beamformers (for a review see [31]). Signals from N input ports are combined with fixed phase relationships to create signals at $\geq N$ output ports. These structures can form beams in one-dimension or in two dimensions [32]. Building Butler combiners with low-loss and well-controlled phases is difficult at millimeter-wavelengths. They would only be suitable for an adding interferometer that uses coherent amplifiers to overcome the beam combiner losses. The Fizeau combiner has lower loss and is more easily scaled to large numbers of inputs. An example of such a system is described in Tucker et al. 2008 and in Section 7.

5.7. Total power detector

The signal from each of the outputs of the combiner is detected (with bolometers if amplifiers are not used) through its total power averaged on time scales given by the time constant of the detector. We assume that the bolometers are background limited, meaning that their noise

variance is proportional to their input power. The power on a given bolometer is then:

$$\mathcal{S}_k = \left\langle \left| \int z_k(\hat{r}) \mathrm{d}\hat{r} \right|^2 \right\rangle_{\mathrm{time}} \quad (7)$$

$$= \int \langle z_k(\hat{r}) z_k^\star(\hat{r}') \rangle_{\mathrm{time}} \, \mathrm{d}\hat{r}\mathrm{d}\hat{r}'. \quad (8)$$

The signals coming from different directions in the sky are incoherent so that their time averaged correlation vanishes:

$$\langle z_k(\hat{r}) z_k^\star(\hat{r}') \rangle_{\mathrm{time}} = \left\langle |z_k(\hat{r})|^2 \right\rangle_{\mathrm{time}} \delta(\hat{r} - \hat{r}') \quad (9)$$

$$\equiv |z_k(\hat{r})|^2 \, \delta(\hat{r} - \hat{r}'). \quad (10)$$

From now on, z is then implicitely replaced by its time-averaged value. The signal on the bolometers is finally:

$$\mathcal{S}_k = \int |z_k(\hat{r})|^2 \, \mathrm{d}\hat{r}. \quad (11)$$

5.8. Stokes parameter visibilities

Developing the signal on the bolometers in terms of the incoming electric fields easily shows autocorrelation terms for each channel as well as cross-correlation terms between all the possible pairs of channels:

$$\mathcal{S}_k = \frac{1}{N_{\mathrm{out}}} \int \left\{ \sum_{i=0}^{N_h - 1} \left| \sum_{\eta=0}^{1} \epsilon_i^\eta(\hat{r}) \exp\left(i \Phi_{k,i}^\eta \right) \right|^2 + 2\mathrm{Re} \left[\sum_{i<j} \sum_{\eta_1, \eta_2} \epsilon_i^{\eta_1}(\hat{r}) \epsilon_j^{\eta_2 \star}(\hat{r}) \exp\left(i(\Phi_{k,i}^{\eta_1} - \Phi_{k,j}^{\eta_2}) \right) \right] \right\} \mathrm{d}\hat{r}. \quad (12)$$

The electric fields from different horns are related through Eq. 2 and introduce the Stokes parameters that are generally used to describe polarized radiation:

$$I = \left\langle \left| E_\parallel \right|^2 \right\rangle + \left\langle |E_\perp|^2 \right\rangle, \quad (13)$$

$$Q = \left\langle \left| E_\parallel \right|^2 \right\rangle - \left\langle |E_\perp|^2 \right\rangle, \quad (14)$$

$$U = \left\langle E_\parallel E_\perp^\star \right\rangle + \left\langle E_\parallel^\star E_\perp \right\rangle = 2\mathrm{Re} \left\langle E_\parallel E_\perp^\star \right\rangle, \quad (15)$$

$$V = i \left(\left\langle E_\parallel E_\perp^\star \right\rangle - \left\langle E_\parallel^\star E_\perp \right\rangle \right) = -2\mathrm{Im} \left\langle E_\parallel E_\perp^\star \right\rangle. \quad (16)$$

The Stokes parameter visibilities are defined as (S stands for I, Q, U or V):

$$\mathsf{V}_S(\vec{u}_\beta) = \int S(\vec{r}) G^2(\hat{r}) \exp(2i\pi \vec{u}_\beta \cdot \hat{r}) \mathrm{d}\hat{r}. \quad (17)$$

The phase-shift differences for a baseline b formed by horns i and j measured in the channel k are:

$$\Delta\Phi_{k,b}^{\parallel\,\parallel} = \Phi_{k,i}^\parallel - \Phi_{k,j}^\parallel, \quad (18)$$

$$\Delta\Phi_{k,b}^{\perp\,\perp} = \Phi_{k,i}^\perp - \Phi_{k,j}^\perp, \quad (19)$$

$$\Delta\Phi_{k,b}^{\parallel\perp} = \Phi_{k,i}^\parallel - \Phi_{k,j}^\perp, \quad (20)$$

$$\Delta\Phi_{k,b}^{\perp\parallel} = \Phi_{k,i}^\perp - \Phi_{k,j}^\parallel. \quad (21)$$

Putting all these definitions into Eq. 12 and after some calculations one finds that the signal on the bolometer k can be expressed purely in terms of the Stokes parameter visibilities and the phase-shifting values (the subscript b stands for all the $N_h(N_h-1)/2$ available baselines and n_k is the noise):

$$\mathcal{S}_k \;=\; \vec{\Lambda}_k \cdot \vec{\mathsf{S}} + \sum_{b=0}^{N_h(N_h-1)/2-1} \vec{\Gamma}_{k,b} \cdot \vec{\mathcal{V}}_b + n_k, \tag{22}$$

where the first term is the autocorrelations of all horns and the second one contains the cross-correlations, hence the interference patterns. That is, the first term contains signals similar to those recovered by a correlation polarimeter, with sampling of the sky given by the beam patterns of the horns. This term allows measurement of large-scale features and hence the low-l portion of the power spectrum. The second term represents the visibilities. We have used the following definitions:

$$\vec{\Lambda}_k = \frac{1}{N_{\rm out}} \sum_{i=0}^{N_h-1} \begin{pmatrix} 1 \\ 0 \\ \cos(\Phi^{\parallel}_{k,i} - \Phi^{\perp}_{k,i}) \\ \sin(\Phi^{\parallel}_{k,i} - \Phi^{\perp}_{k,i}) \end{pmatrix}, \; \vec{\mathsf{S}}^t = \begin{pmatrix} \int I(\vec{n}) B^2(\vec{n}) \mathrm{d}\vec{n} \\ \int Q(\vec{n}) B^2(\vec{n}) \mathrm{d}\vec{n} \\ \int U(\vec{n}) B^2(\vec{n}) \mathrm{d}\vec{n} \\ \int V(\vec{n}) B^2(\vec{n}) \mathrm{d}\vec{n} \end{pmatrix}, \tag{23}$$

$$\vec{\Gamma}_{k,b} = \frac{1}{N_{\rm out}} \begin{pmatrix} \cos\Delta\Phi^{\parallel\,\parallel}_{k,b} + \cos\Delta\Phi^{\perp\perp}_{k,b} \\ -(\sin\Delta\Phi^{\parallel\,\parallel}_{k,b} + \sin\Delta\Phi^{\perp\perp}_{k,b}) \\ \cos\Delta\Phi^{\parallel\,\parallel}_{k,b} - \cos\Delta\Phi^{\perp\perp}_{k,b} \\ -(\sin\Delta\Phi^{\parallel\,\parallel}_{k,b} - \sin\Delta\Phi^{\perp\perp}_{k,b}) \\ \cos\Delta\Phi^{\parallel\perp}_{k,b} + \cos\Delta\Phi^{\perp\parallel}_{k,b} \\ -(\sin\Delta\Phi^{\parallel\perp}_{k,b} + \sin\Delta\Phi^{\perp\parallel}_{k,b}) \\ -(\sin\Delta\Phi^{\parallel\perp}_{k,b} - \sin\Delta\Phi^{\perp\parallel}_{k,b}) \\ -(\cos\Delta\Phi^{\parallel\perp}_{k,b} - \cos\Delta\Phi^{\perp\parallel}_{k,b}) \end{pmatrix}, \; \vec{\mathcal{V}_b}^{\,t} = \begin{pmatrix} \mathrm{Re}\left[\mathsf{V}_I(\vec{u}_b)\right] \\ \mathrm{Im}\left[\mathsf{V}_I(\vec{u}_b)\right] \\ \mathrm{Re}\left[\mathsf{V}_Q(\vec{u}_b)\right] \\ \mathrm{Im}\left[\mathsf{V}_Q(\vec{u}_b)\right] \\ \mathrm{Re}\left[\mathsf{V}_U(\vec{u}_b)\right] \\ \mathrm{Im}\left[\mathsf{V}_U(\vec{u}_b)\right] \\ \mathrm{Re}\left[\mathsf{V}_V(\vec{u}_b)\right] \\ \mathrm{Im}\left[\mathsf{V}_V(\vec{u}_b)\right] \end{pmatrix}. \tag{24}$$

All of this can be regrouped as a simple linear expression involving a vector with all the sky information (Stokes parameter autocorrelations $\vec{\mathsf{S}}$ and all visibilities $\vec{\mathcal{V}_b}$) labelled $\vec{X}$ and another involving the phase-shifting informations ($\vec{\Lambda}_k$ and $\vec{\Gamma}_{k,b}$) labelled $\vec{A}_k$:

$$\mathcal{S}_k \;=\; \vec{A}_k \cdot \vec{X} + n_k. \tag{25}$$

Finally, various measurements of the signal coming from the different channels and/or from different time samples with different phase-shifting configurations can be regrouped together by adding columns to $\vec{A}$ which then becomes a matrix A and transforming the individual measurement $\mathcal{S}_k$ into a vector $\vec{\mathcal{S}}$:

$$\vec{\mathcal{S}} \;=\; A \cdot \vec{X} + \vec{n}. \tag{26}$$

The sky signals are recovered by solving this equation for $\vec{X}$ using techniques familiar from CMB map-making. The sensitivity of an adding interferometer that uses bolometers as detectors has been calculated in detail [30]. The bolometric interferometer has sensitivity comparable to that of an imaging system that uses bolometers and couples to the same number of modes on the sky (i.e. that has the number of detectors equal to the number of antennas in the interferometer array).

6. Adding Interferometry: Systematic Effects and Challenges

Some of the advantages of interferometry for controlling systematic effects were discussed in Section 2. Here we focus on some systematic effects and challenges that are specific to adding interferometers.

Phase modulation: Perhaps the most significant technical challenge for the adding interferometer is the phase modulator. The difference in loss in the different phase states must be small and stable or else the phase modulation will couple a portion of the total power signal on the bolometers into Q, U, and V.

[29] show the importance of choosing a modulation sequence that reads out redundant baselines simultaneously. For large arrays the number of steps in the switching sequence can become very large. In order to cycle through the full sequence faster than the 1/f knee in the detector response requires rapid phase modulation ($\sim$1 kHz) and hence detectors with short time constants.

Bandwidth smearing: The sensitivity of a receiver to broadband signals increases as the square root of the bandwidth. For interferometers, the bandwidth restricts the angular range, θ, over which fringes are detected [33] ; [34]. If we assume the path lengths for a source at the center of the FOV are equal, then the path length difference for a source at an angle θ from the center along the baseline axis is θB, where B is the baseline distance. If this path length difference is small compared to the coherence length of the light, $\lambda^2/\Delta\lambda$, then the fringe contrast is not affected. Thus the FOV is determined by $\theta_{\rm FOV} \leq (\lambda/\Delta\lambda)(\lambda/B)$. This equation indicates that for angles of the order of the product of the spectral resolution times the angular resolution, the fringe smearing is important. This relation imposes restrictions on the ratio between the maximum baseline achievable by the interferometer and the spectral bandwidth of the receiver. A bandwidth of 15% sets the maximum baseline to about 6 times the diameter of each antenna.

Simulations: Adding interferometers are different enough from imaging systems that simulations are required to answer many questions. Currently there is one such simulation under development, at APC at University of Paris VII [29]. This tool is currently capable of simulating the recovery of the Stokes parameter visibilities for realistic adding interferometer designs that incorporate a Fizeau beam combiner. The following design parameters can be adjusted: number and location of the input antennas (horns) in the aperture plane, number and location of the detectors in the "fringe plane," the phase shifter sequences used for recovering the visibilities, and the focal length of the Fizeau combiner. Bandwidth effects such as those mentioned above are now being included. Studies that could be carried out include effects of asymmetric beam patterns on the sky, low-frequency stability, spectral band shape, cross-talk between antenna, calibration, instrumental polarization, etc.

Fringe rotation: Interferometers with independently mounted, tracking antennas (like VLA or SZA) enjoy a modulation of the signal caused by the rotation of the earth. This modulation is different for sources in the sky than for sources on the ground and provides a powerful tool for interferometers to reject ground-spill. On the other hand, co-mounted interferometers (DASI and CBI) do not have this advantage. Large arrays with $\sim$ 100's of antennas will almost certainly have to be co-mounted.

Cross-coupling: Some coupling between the antennas in a close-packed array will occur. This effect will lead to correlated signals that will be modulated by the phase modulators, and hence to an offset in the demodulated signals. DASI used cylindrical baffles around its horn antennas to reduce the cross-coupling. Further study is needed to determine the implications of this systematic effect.

7. EPIC Mission Concept Study

The EPIC mission concept study for the Einstein Inflation Probe focused on the possibility of using a bolometric adding interferometer. Figure 3 shows a possible configuration for a

bolometric interferometer module for EPIC. The array views the sky through a close-packed cluster of corrugated horn antennas. The two polarizations (either linear or circular) are split by an ortho-mode transducer and individually phase-modulated (Fig. 4). The beams are then combined with a Fizeau combiner in the form of a cold, compact, on-axis Cassegrain telescope. Interference fringes formed by the various antenna baselines appear on the bolometer array in the focal plane of the telescope. The superimposed fringes are separated from each other using a phase modulation sequence that uniquely encodes each visibility (Figs. 5, 6). A prototype, the Millimeter-wave Bolometric Interferometer (MBI) has been constructed and is undergoing testing [35].

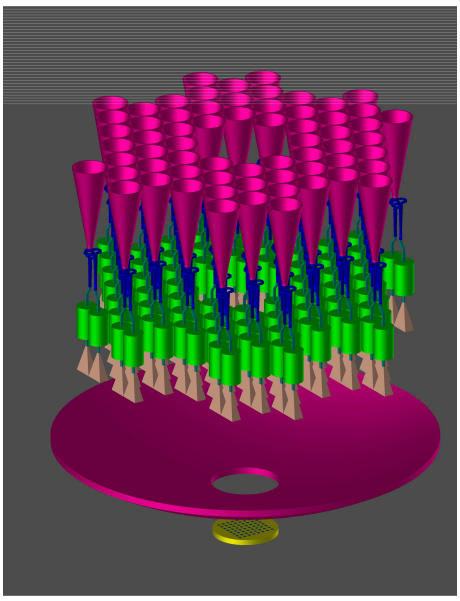

Figure 3. A three-dimensional view of 64 corrugated horn antennas arranged in a close-packed array illuminating a Fizeau combiner. The detector array sits behind the primary mirror of the beam combiner. Note that the distances between the antennas, primary mirror and detector array are not to scale. EPIC could be made of a cluster of these fundamental modules, with multiple copies operating at frequencies from 30 GHz to 300 GHz

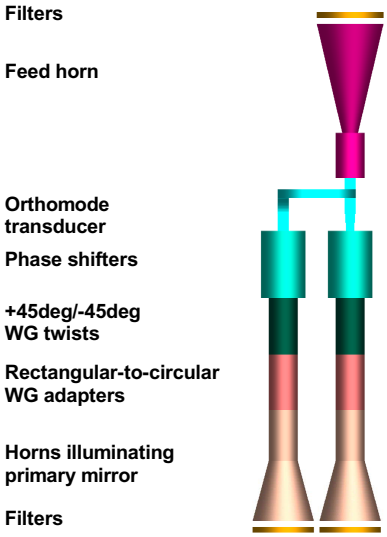

Figure 4. Input unit (IU) of the EPIC interferometer. The two polarizations are separated using an orthomode transducer and are rotated in waveguide (WG) so that the two polarization vectors are aligned. A $\pm 90°$ phase modulation is introduced in one of the arms and the two signals are directed at the Fizeau combiner. The interference of the two signals from an IU results in a correlation receiver, instantaneously sensitive to the Stokes U parameter. The interference of signals from different IUs results in an interferometer.

The EPIC mission concept includes multiple close-packed arrays of horn antennas that are co-aligned and pointed directly at the sky, with no intervening lenses or reflectors. Each array is configured as an adding interferometer using the beam combination scheme of Figure 3. The interferometer measures the visibilities from all baselines in the array. In addition, the phase modulators can be operated in such a way that the signals from each antenna interfere with themselves. In this mode the system acts as an array of correlation polarimeters, sensitive to Q and U averaged over a single antenna beam. The correlation polarimeter mode is used to measure the lowest spherical harmonics, while the interferometric mode recovers the higher-order multipoles. Both of these modes can operate simultaneously.

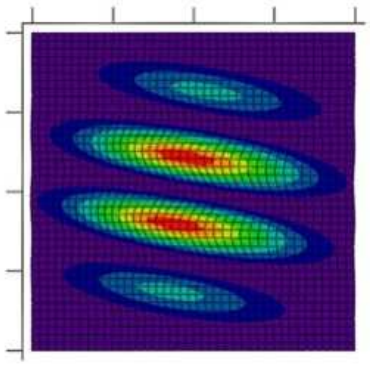

Figure 5. Simulation of fringe patterns formed in the focal plane of the Fizeau beam combiner from a single baseline.

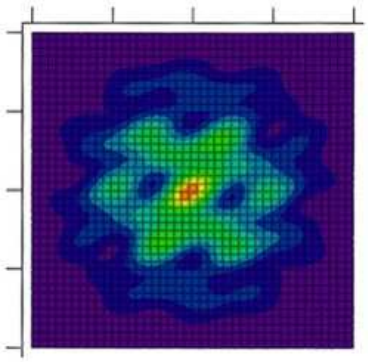

Figure 6. Superposition of fringes from 6 baselines (as expected in MBI). Fringes are separated by phase modulation sequence.

In an interferometer, each individual pointing covers a large sky area and samples many different baselines simultaneously, potentially reducing systematic errors in map-making. The relatively simple configuration of the EPIC instrument may allow for an additional degree of freedom in the scan using rotation of the instrument. If the low-l modes are recovered by using the instrument in a correlation receiver configuration, then scan-strategy issues similar to those of an imaging system may arise.

Figure 7 displays the sensitivity for one possible configuration under study for EPIC. There is a total of 16 arrays, each including 64 close-packed corrugated horn antennas, for a total of 1024 horns. Each horn has a beam width of 15°. Each array operates in wide bands (∼20%) centered at frequencies between ∼30–300 GHz. There are 8 arrays sensitive to 90 GHz, the primary science channel. The other 8 arrays are for measuring and removing foregrounds; they are not included in the sensitivity estimate. The instrument and observing patterns have not been optimized. The exact band placements and number of bands will be chosen to optimize the removal of foreground contamination. The detectors are cold (∼100 mK), background-limited superconducting transition-edge sensors (TES) read out by SQUID multiplexers. The instrument efficiency is taken to be 50%. Emission from the cryostat window dominates the optical loading on the detectors. EPIC surveys the full sky with a combination of instrument rotation and precession.

8. Technologies and Readiness

Although no adding interferometers have been used for CMB measurements the technologies required for building such an instrument are not very different from those required for imaging systems. We list here the critical components and some of the required specifications. See Table 3. Most of these components are discussed in more detail in other white papers for this workshop.

Horn arrays: Close-packed horn antenna arrays with $\sim$ 100 elements are required for each wavelength, from $\sim$ 30 GHz to 300 GHz. Lightweight platelet arrays of corrugated horns are an attractive option. Recent developments in smooth-walled horns (similar to Potter horns) may offer comparably symmetric beams with low sidelobes with lower mass and easier fabrication.

Phase modulators: As mentioned above, these components are critical to the success of adding interferometry. Differential loss between the different phase states must be small and stable to reject the total power signal on the bolometers. Rapid switching and settling is necessary to accommodate long switching sequences. Low power dissipation is also required. Ferrite rotation

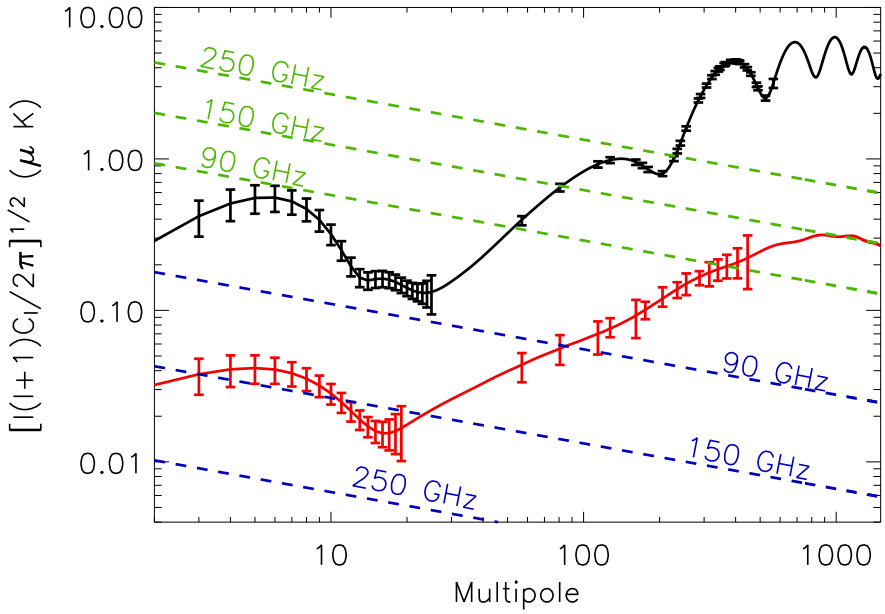

Figure 7. Expected sensitivity of EPIC, a mission concept for the Einstein Inflation Probe, to E (black) and B (red) polarization. The power spectra are based on the best-fit model from *WMAP* [36]. The tensor-to-scalar ratio is taken to be 0.01. Errors (1σ) assume one year of integration sampling the full sky uniformly. The estimates are representative of the capabilities of possible designs for the CMBPol. The configuration assumed here includes 1024 feed horns, with 512 sensitive to 90 GHz, the primary science channel; the other 512 feed horns are for measuring and removing foregrounds and are not included in this estimate. The dotted lines show the expected levels of polarized dust emission and the dashed lines show the expected levels of polarized synchrotron emission at 90 GHz, 150 GHz and 250 GHz based on the WMAP results [37]. EPIC operates both as an imaging instrument and an interferometer; low-l points come from operating the interferometer as single-beam correlation radiometers while high-l points come from operating the instrument as an interferometer.

modulators [35] are one possibility. Another is MEMs devices.

Beam combiners: At millimeter wavelengths only quasi-optical beam combiners offer low enough loss to be used with bolometric detectors. Guided wave combiners are suitable for adding interferometers with amplifiers.

Detectors : For bolometric adding interferometers, bolometer arrays operating at the background limit are required. Because the number of detectors for each interferometer $\sim 4\times N_h$, the power loading on each bolometer is $\sim 1/4$ the loading from a single mode looking at the CMB. Hence, detector noise must be even lower than for bolometers used for imaging systems. Arrays of ~ 400 detectors are required. In order to capture all of the radiation arriving at the fringe plane, these must be absorber-coupled detectors. An excellent example would be the BUG arrays developed for GISMO.

9. Conclusion

Adding interferometry is a viable approach to B-mode searches and offers an attractive alternative to imaging techniques. The most critical technology in need of development is phase modulation. The other necessary technologies are similar to those required for CMB imaging systems.

Table 3. Technology Readiness Levels for Adding Interferometers

Component	*TRL*	*Heritage*
Corrugated horn antennas	9	WMAP & COBE
OMT	9 (<100 GHz)	WMAP
Phase modulator	6 (< 100 GHz)	BICEP & MBI
Fizeau combiner	5	MBI
Focal Plane Arrays		
NTD Ge bolometers	8	Planck & Herschel
TES bolometers	6	SCUBA, GBT, EBEX
LHe cryostat	9	Spitzer, ISO, Herschel, COBE
Sub-K cooler: single-shot ADR	9	ASTRO-E2

Acknowledgments
We thank the members of the MBI and BRAIN collaboration, who are responsible for most of the ideas presented here.

References

[1] Kovac J M, Leitch E M, Pryke C, Carlstrom J E, Halverson N W and Holzapfel W L 2002 *Nature* **420** 772–787 (*Preprint* `astro-ph/0209478`)

[2] Timbie P T, Tucker G S, Ade P A R, Ali S, Bierman E, Bunn E F, Calderon C, Gault A C, Hyland P O, Keating B G, Kim J, Korotkov A, Malu S S, Mauskopf P, Murphy J A, O'Sullivan C, Piccirillo L and Wandelt B D 2006 *New Astronomy Review* **50** 999–1008

[3] Birkinshaw M 1999 *Physics Reports* **310** 97–195 (*Preprint* `astro-ph/9808050`)

[4] Carlstrom J E, Holder G P and Reese E D 2002 *ARA &A* **40** 643–680 (*Preprint* `astro-ph/0208192`)

[5] Loh M, Carlstrom J E, Cartwright J K, Greer C, Hawkins D, Hennessy R, Joy M, Lamb J, Leitch E, Miller A, Mroczkowski T, Muchovej S, Pryke C, Reddall B, Richardson G, Runyan M, Sharp M and Woody D 2005 *American Astronomical Society Meeting Abstracts* **207** 41.01–+

[6] Baker J C, Grainge K, Hobson M P, Jones M E, Kneissl R, Lasenby A N, O'Sullivan C M M, Pooley G, Rocha G, Saunders R, Scott P F and Waldram E M 1999 *MNRAS* **308** 1173–1178 (*Preprint* `astro-ph/9904415`)

[7] Dickinson C, Battye R A, Carreira P, Cleary K, Davies R D, Davis R J, Genova-Santos R, Grainge K, Gutiérrez C M, Hafez Y A, Hobson M P, Jones M E, Kneissl R, Lancaster K, Lasenby A, Leahy J P, Maisinger K, Ödman C, Pooley G, Rajguru N, Rebolo R, Rubiño-Martin J A, Saunders R D E, Savage R S, Scaife A, Scott P F, Slosar A, Sosa Molina P, Taylor A C, Titterington D, Waldram E, Watson R A and Wilkinson A 2004 *MNRAS* **353** 732–746 (*Preprint* `astro-ph/0402498`)

[8] Halverson N W, Leitch E M, Pryke C, Kovac J, Carlstrom J E, Holzapfel W L, Dragovan M, Cartwright J K, Mason B S, Padin S, Pearson T J, Readhead A C S and Shepherd M C 2002 *ApJ* **568** 38–45 (*Preprint* `astro-ph/0104489`)

[9] Readhead A C S, Mason B S, Contaldi C R, Pearson T J, Bond J R, Myers S T, Padin S, Sievers J L, Cartwright J K, Shepherd M C, Pogosyan D, Prunet S, Altamirano P, Bustos

R, Bronfman L, Casassus S, Holzapfel W L, May J, Pen U L, Torres S and Udomprasert P S 2004 *ApJ* **609** 498–512 (*Preprint* astro-ph/0402359)

[10] Leitch E M, Kovac J M, Halverson N W, Carlstrom J E, Pryke C and Smith M W E 2005 *ApJ* **624** 10–20 (*Preprint* astro-ph/0409357)

[11] Readhead A C S, Myers S T, Pearson T J, Sievers J L, Mason B S, Contaldi C R, Bond J R, Bustos R, Altamirano P, Achermann C, Bronfman L, Carlstrom J E, Cartwright J K, Casassus S, Dickinson C, Holzapfel W L, Kovac J M, Leitch E M, May J, Padin S, Pogosyan D, Pospieszalski M, Pryke C, Reeves R, Shepherd M C and Torres S 2004 *Science* **306** 836–844 (*Preprint* astro-ph/0409569)

[12] Cartwright J K, Pearson T J, Readhead A C S, Shepherd M C, Sievers J L and Taylor G B 2005 *ApJ* **623** 11–16 (*Preprint* astro-ph/0502174)

[13] Goldsmith P F 1998 *Quasioptical Systems* (IEEE Press)

[14] Hu W, Hedman M M and Zaldarriaga M 2003 *Phys. Rev. D* **67** 043004–+ (*Preprint* astro-ph/0210096)

[15] Knox L and Song Y S 2002 *Phys. Rev. Lett.* **89** 011303–+ (*Preprint* astro-ph/0202286)

[16] White M, Carlstrom J E, Dragovan M and Holzapfel W L 1999 *ApJ* **514** 12–24 (*Preprint* astro-ph/9712195)

[17] Carretti E, Tascone R, Cortiglioni S, Monari J and Orsini M 2001 *New Astronomy* **6** 173–187 (*Preprint* astro-ph/0103318)

[18] Carretti E, Cortiglioni S, Sbarra C and Tascone R 2004 *A &A* **420** 437–445 (*Preprint* astro-ph/0403493)

[19] Hanany S and Marrone D P 2002 *Appl. Opt.* **41** 4666–4670 (*Preprint* astro-ph/0206211)

[20] Leitch E M, Kovac J M, Pryke C, Carlstrom J E, Halverson N W, Holzapfel W L, Dragovan M, Reddall B and Sandberg E S 2002 *Nature* **420** 763–771 (*Preprint* astro-ph/0209476)

[21] Bunn E F 2007 *Phys. Rev. D* **75** 083517–+ (*Preprint* arXiv:astro-ph/0607312)

[22] Lewis A, Challinor A and Turok N 2002 *Phys. Rev. D* **65** 023505–+ (*Preprint* astro-ph/0106536)

[23] Bunn E F 2003 *New Astronomy Review* **47** 987–994 (*Preprint* astro-ph/0306003)

[24] Park C G, Ng K W, Park C, Liu G C and Umetsu K 2003 *ApJ* **589** 67–81 (*Preprint* astro-ph/0209491)

[25] Park C G and Ng K W 2004 *ApJ* **609** 15–21 (*Preprint* astro-ph/0304167)

[26] Conway J E, Cornwell T J and Wilkinson P N 1990 *MNRAS* **246** 490–+

[27] Rohlfs K and Wilson T L 2004 *Tools of Radio Astronomy* (Springer)

[28] Zmuidzinas J 2003 *Optical Society of America Journal A* **20** 218–233

[29] Charlassier R, Hamilton J C, Bréelle É, Ghribi A, Giraud-Héraud Y, Kaplan J, Piat M and Prêle D 2008 *ArXiv e-prints* **806** (*Preprint* 0806.0380)

[30] Hamilton J C, Charlassier R, Cressiot C, Kaplan J, Piat M and Rosset C 2008 *ArXiv e-prints* **807** (*Preprint* 0807.0438)

[31] Hall P S and Veterlein S J 1990 *Inst. Elect. Eng. Proc.* **137** 293–303

[32] Remez J, Segal A and Shansi R 2005 *IEEE Antennas Wireless Propag. Letters* **4** 293–296

[33] Thompson A R, Moran J M and Swenson Jr G W 2001 *Interferometry and Synthesis in Radio Astronomy, 2nd Edition* (Interferometry and synthesis in radio astronomy by A. Richard Thompson, James M. Moran, and George W. Swenson, Jr. 2nd ed. New York : Wiley, c2001.xxiii, 692 p. : ill. ; 25 cm. "A Wiley-Interscience publication." Includes bibliographical references and indexes. ISBN : 0471254924)

[34] Böker T and Allen R J 1999 *ApJS* **125** 123–142 (*Preprint* arXiv:astro-ph/9903490)

[35] Tucker G S, Korotkov A L, Gault A C, Hyland P O, Malu S, Timbie P T, Bunn E F, Keating B G, Bierman E, OSullivan C, Ade P A R and Piccirillo L 2008 *Millimeter and Submillimeter Detectors and Instrumentation for Astronomy IV. Edited by Zmuidzinas, Jonas; Holland, Wayne S.; Withington, Stafford; Duncan, William D. to appear in Proceedings of the SPIE (2008).* Presented at the Society of Photo-Optical Instrumentation Engineers (SPIE) Conference

[36] Page L, Hinshaw G, Komatsu E, Nolta M R, Spergel D N, Bennett C L, Barnes C, Bean R, Doré O, Dunkley J, Halpern M, Hill R S, Jarosik N, Kogut A, Limon M, Meyer S S, Odegard N, Peiris H V, Tucker G S, Verde L, Weiland J L, Wollack E and Wright E L 2007 *ApJS* **170** 335–376 (*Preprint* arXiv:astro-ph/0603450)

[37] Spergel D N, Bean R, Doré O, Nolta M R, Bennett C L, Dunkley J, Hinshaw G, Jarosik N, Komatsu E, Page L, Peiris H V, Verde L, Halpern M, Hill R S, Kogut A, Limon M, Meyer S S, Odegard N, Tucker G S, Weiland J L, Wollack E and Wright E L 2007 *ApJS* **170** 377–408 (*Preprint* arXiv:astro-ph/0603449)